Precision measurement of the isospin dependence in the 2N and 3N short range correlation region

J. Arrington (co-spokesperson), P. Solvignon (co-spokesperson and contact), D. F. Geesaman, K. Hafidi, R. Holt, P. Reimer
Argonne National Laboratory, Argonne, IL 60439

D. B. Day (co-spokesperson), H. Baghdasaryan, N. Kalantarians
University of Virginia, Charlottesville, VA, 22901

F. Benmokhtar
Carnegie Mellon University, Pittsburgh, PA 15213

A.T. Katramatou and G.G. Petratos
Kent State University, Kent, OH 44242

W. Bertozzi, S. Gilad
Massachusetts Institute of Technology, Cambridge, MA 02139

R. Ransome
Rutgers, the State University of New Jersey, Piscataway, NJ 08854

E. Piasetzky, I. Pomerantz, G. Ron
Tel Aviv University, Tel Aviv, 69978 Israel

D. Higinbotham, V. Sulkosky , D. Gaskell
Thomas Jefferson National Accelerator Facility, Newport News, VA 23606

E. J. Beise
University of Maryland, College Park, MD 20742

K. Slifer
University of New Hampshire, Durham, NH 03823

N. Fomin
University of Tennessee, Knoxville, TN 37996

and

The Hall A Collaboration

Abstract

We propose to perform a precision test of the isospin dependence of two-nucleon short range correlations using mirror nuclei: ^{3}He and ^{3}H. We will also extend the cross section ratio measurement to the $x > 2$ region where three-nucleon short range correlations dominate; This will constitute the first test of the isospin dependence of three-nucleon clusters. An unpolarized electron beam of 4.4 GeV, the under-design room temperature ^{3}He and ^{3}H target system and both high resolution spectrometers (HRS) in standard electron detection configuration are needed for our proposed measurement. The ^{3}H target is "conditionally approved" as in E06-12-118. The proposed measurement requires 13 days of beam time including calibration, overhead, and background measurements.

I. INTRODUCTION TO SHORT RANGE CORRELATIONS

Short-Range correlations (SRCs) have been recognized as responsible for the high momentum tail of the nucleon momentum distribution in nuclei. In the dense enclosure of nuclei, the attractive core produces overlaps between nucleon wavefunctions, and the strong short-range repulsive force induces potentially high momenta to the overlapping nucleons.

Measurements of the spectroscopic strengths for the nuclear valence orbitals by the (e,e'p) reactions [1] exhibit a 30-40% missing strength compared to the mean field expectation (see Fig. 1). This discrepancy was attributed in part to the non-negligible SRC pieces in the nuclear wavefunction. In the shell model, the short range repulsive force is not taken into account. This leads to a significant excess in the nuclear cross section due to large increase in the non-single particle reactions with nucleon momenta well above the Fermi momentum k_F.

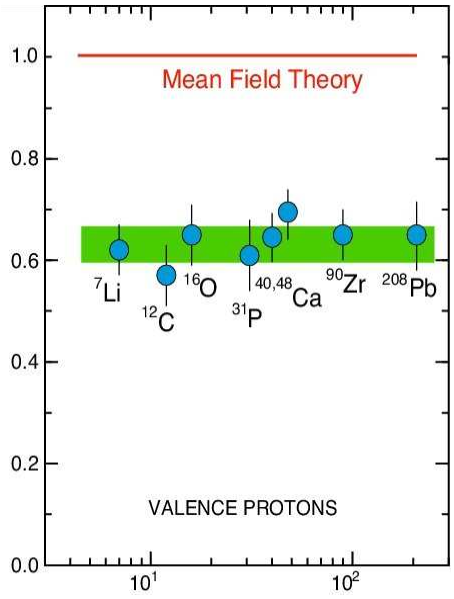

FIG. 1: Quasi-particle strength for valence orbitals. Figure reproduced from [1].

While single nucleon knockout reactions A(e,e'p) allow us to look at the shell model contributions, it is much more difficult to probe the high-momentum nucleons generated by correlations, as the cross section in this region has large contributions from other processes such as final-state interactions and meson-exchange currents. Inclusive electron scattering at $x > 1$ can be used to probe these high-momentum nucleons, providing cleaner measurements that complement the more detailed measurements possible in coincidence reactions.

By choosing the kinematic region where the nucleon momentum is well above the Fermi momentum, the cross section will be dominated by the scattering on high momentum nucleons belonging to short-range correlations. For a free nucleon, the Bjorken variable x ranges from 0 to 1. For nuclei, $x > 1$ implies that more than one nucleon are involved in the scattering. However, near $x = 1$, where quasi-elastic scattering dominates the reaction, simple Fermi motion broadens the quasi-elastic peak, extending the strength of the single particle reaction till about $x = 1.3$. This means that, in a nucleus of A nucleons, the region in Bjorken x where SRC dominates extends from $x = 1.3$ to close to the elastic limit ($x = A$).

As it would be expected for scattering on a tighly bound system, scaling behavior in the nuclear cross sections is expected to manifest in the $x > 1.3$ region. Frankfurt and Strikman [2, 3] showed that the cross section for $x \gtrsim 1.3$ (where the single particle contribution is negligible) can be written as a sum of contributions from 2N, 3N,...

correlations,

$$\sigma_A(x,Q^2) = \sum_{j=2}^{A} \frac{A}{j} a_j(A)\tilde{\sigma}_j(x,Q^2) \quad (1)$$
$$= \frac{A}{2}a_2(A)\tilde{\sigma}_2(x,Q^2) + \frac{A}{3}a_3(A)\tilde{\sigma}_3(x,Q^2) + ...,$$

where $\tilde{\sigma}_j$ is the cross section for scattering from a j-nucleon correlation. The constants $a_j(A)$ are proportional to the probability of finding a nucleon in a j-nucleon correlation. These constants should fall rapidly with j as nuclei are dilute. In this model, the isospin dependence of the SRCs is neglected (as it is throughout Section I). Taking $a_j(A) = 1$ for $A = j$, i.e. defining $a_2(A)$ to be probability of finding a 2N-SRC in nucleus A relative to deuterium, the cross section σ_j reduces to the cross section for scattering from a nucleus with $A = j$, e.g. for $A = 2$, $\sigma_{eD}(x,Q^2) = a_2(A)\sigma_2(x,Q^2) = \sigma_2(x,Q^2)$, with $\sigma_j(x,Q^2) = 0$ for $x > j$.

In the region where 2N-SRCs dominate, the SRC model predicts scaling of the cross section ratio:

$$(2/A)\sigma_A(x,Q^2)/\sigma_D(x,Q^2) = a_2(A)/a_2(D) = a_2(A), \quad (2)$$

where the factor $(2/A)$ yields the ratio of cross sections per nucleon. Thus, for all values of x and Q^2 where the scattering is dominated by 2N-SRCs, the ratio of the cross section from a heavy nucleus to deuterium (or in fact the ratio of any two nuclei) should be independent of x and Q^2, and be a direct measure of the relative number of 2N-SRCs in the nuclei. While this neglects the effects of FSI, it has been argued [4] that in these small-sized SRCs, the FSI is confined to the nucleons in the correlation itself , and should cancel in the ratio. Similar scaling should be observed in the ratio $A/^3$He in the region where scattering from 3N-SRCs dominates. The SRC model outlined here assumes isospin independence and that the CM of the correlation is at rest.

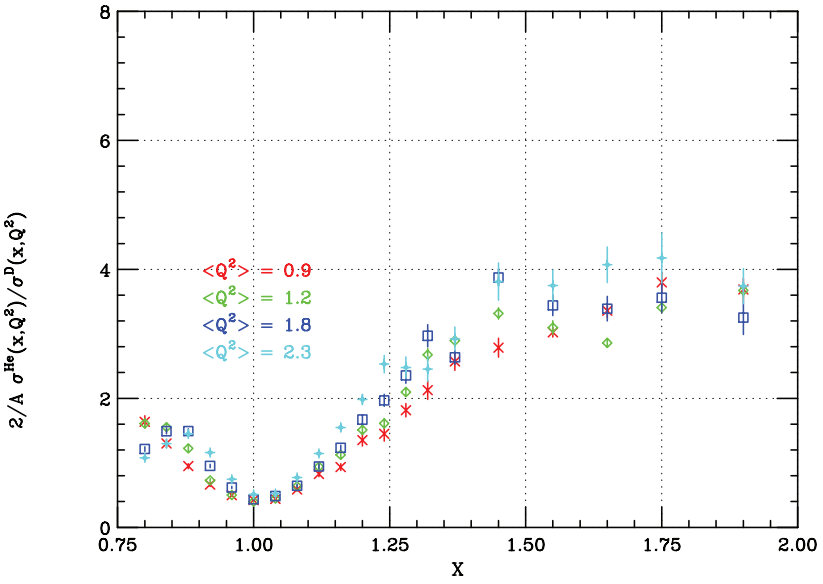

FIG. 2: Evidence of 2N SRC in the cross section ratio of ^{4}He over deuterium from SLAC data [5].

This scaling behavior for 2N-SRCs was first observed in SLAC data [3, 5]. Figure 2 shows the SLAC results on the cross section ratios of ^{4}He over deuterium at several average Q^2. A plateau can be seen at most of the averaged Q^2 for $x > 1.4$. This is a clear signature of scattering off a strongly correlated pair of nucleons. Scaling seems to get better at high Q^2, as long as the inelastic contribution is still negligible at $x > 1$, but this observation is limited by the statistics. More recently in Hall C and Hall B at Jefferson Lab [6, 7], the same high x scaling behavior was

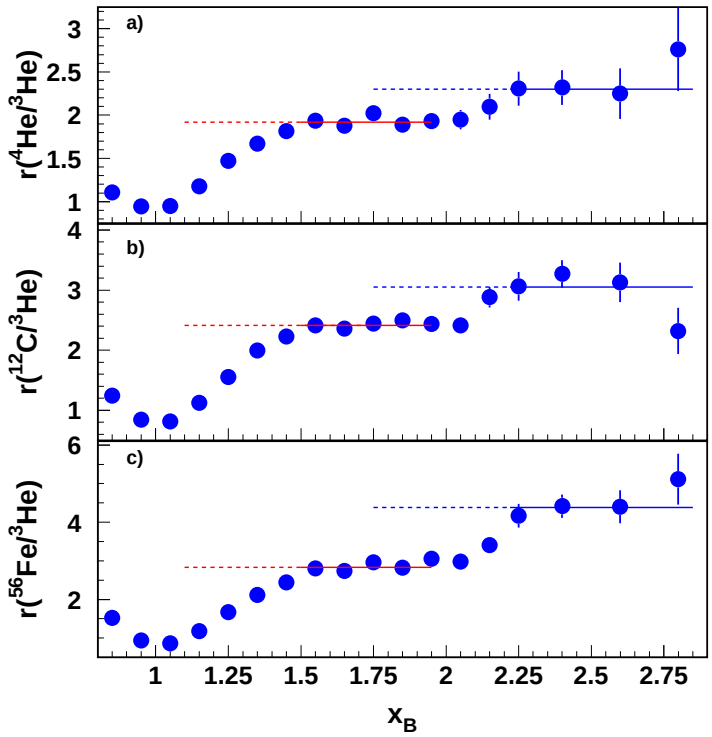

FIG. 3: 2N and 3N correlations from recent JLab Hall B data [7]. The quantities $r(\mathrm{A}/^3\mathrm{He})$ represent the per-nucleon isoscalar cross section ratios.

observed. Moreover, the results from CLAS [7] provided the first direct indication of scaling in the x-region between 2.25 and 2.80, corresponding to dominance of three-nucleon short range correlations, as shown in Figure 3. But these data have limitations that make it difficult to perform a quantitative extraction of the 3N-SRC probabilities, or even to ensure that the measurement is directly sensitive to the 3N-SRC contributions. In this analysis, it is assumed that the onset of scaling for 2N and 3N-SRC happens at the same Q^2, and consequently, all data above this Q^2-value are averaged in order to improve the precision. The statistics are such that there is no real verification of the Q^2-independence of the ratio, and in fact, some indication of a lack of scaling. More precise data, especially at somewhat larger Q^2, are needed to precisely determine 3N-SRC probabilities $a_3(\mathrm{A}/^3\mathrm{He})$ and to clarify its Q^2 and x dependence. Experiment E08-014 [8] is expected to take high precision data in the 3N-SRC region for a Q^2-range 0.8-2.8 $(\mathrm{GeV/c})^2$ in Spring 2011 in Hall A at JLab allowing a more accurate extraction of the 3N-SRC probabilities. For E08-014, the experimenters will map out, in detail, the range were the SRC model and analysis of Fig. 3 are valid.

All the above assumed isospin symmetry in the correlation structure. The new two-nucleon knockout measurements [9, 10] suggest a large difference in "pp" and "pn" pairs. The goal here is to make a more precise, quantitative extraction of the ratio in the 2N SRC region.

II. ISOSPIN DEPENDENCE OF SRC

In the SRC model [2, 3], the nucleon correlations are assumed isospin independent. However recent results from the Hall A two-nucleon knockout experiment E01-015 [10, 11] suggested that the correlated pairs were dominated by np, and that both pp and nn correlations together accounted for only 10% of the total SRCs measured, as shown on Fig. 4. They find that of the 20% contribution to the cross section from the 2N-SRC, 18% are np-pairs and only

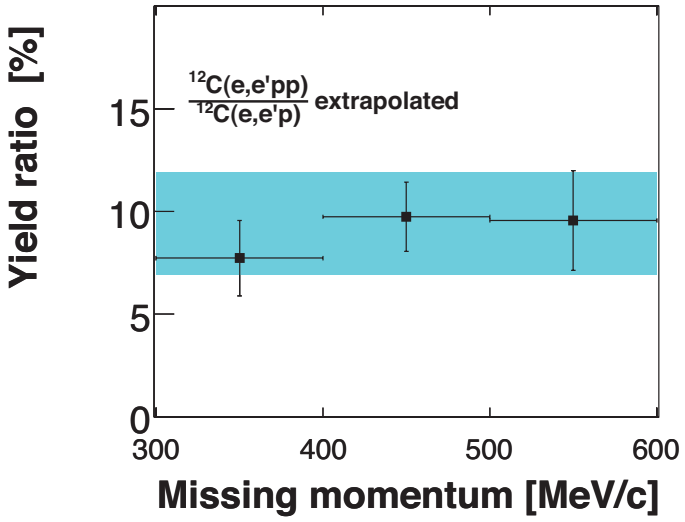

FIG. 4: Results from [10] showing the low probability that the knockout proton originated from a correlated pp pairs.

1% for each pp and nn pairs. This strong isospin dependence was previously derived from combined inclusive and A(p,ppn) reactions [12].

Recent calculations [13] show that for 2N-SRCs at rest in a nucleus, the tensor force yields an excess of high-momentum nucleons in deuteron-like (T=0) np correlations, while nn, pp, np pairs with T=1 are all strongly suppressed. Their calculation for ^{4}He is shown in Fig. 5. For comparison the scaled momentum distribution for the AV18 deuteron is plotted, as well as its S- and D-wave components. This clearly demonstrates the dominance of the tensor part in the momentum range 1.4-4.0 fm^{-1} where the correlated pairs are expected to dominate the nuclear wave function.

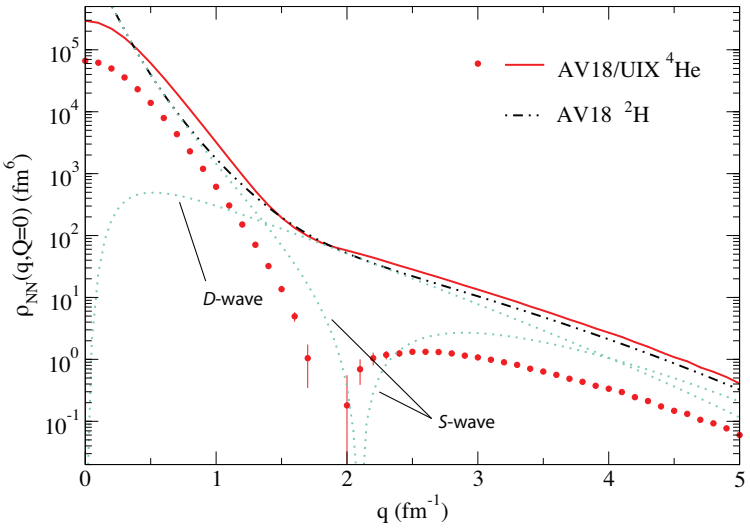

FIG. 5: Calculations from [13]. The red line represents the np pair relative momentum distribution and the red symbols the pp pair relative momentum distribution obtained with fully realistic AV18/UIX hamiltonian. Also shown is the scaled momentum distribution for the AV18 deuteron and its separate S- and D-wave components (dotted lines).

The experiment E01-015 is kinematically complete and can therefore determine the approximate region of the momentum distribution being probed, within the impulse approximation. However effects from FSI, MEC, ... make

it difficult to extract a precise quantitative measure of this isospin asymmetry. Inclusive scattering can provide a cleaner extraction on the isospin dependence which will complement the two-nucleon knockout interpretation.

While the ratios shown in Fig. 3 are corrected for the difference between the electron-proton and electron-neutron cross sections, they assume that the ratio of neutrons to protons in the 2N-SRCs and 3N-SRCs is equal to the N/Z ratio of the nucleus. We can study these effects using inclusive scattering in the 2N-SRC (or 3N-SRC) dominated regions for nuclei with different N/Z ratios. Detailed calculations exist for few-body nuclei, and it is easy to see the impact of the isospin dependence for the simpliest case; the comparison of ^{3}He and ^{3}H. For isospin-independent 2N-SRCs, ^{3}He will have two pn pairs and one pp pair, compared to two pn pairs and one nn pair for ^{3}H. For ^{3}He, this yields four options for a high-momentum proton and two for a high-momentum neutron, yielding a proton distribution that is twice the neutron distribution at large momenta. For ^{3}H, the opposite happens, but in both cases, the ratio of the proton to neutron momentum distributions, $n_p(k)/n_n(k)$ at high momentum is just equal to the Z/N ratio. If deuteron-like SRCs dominate, then each nucleus has two pn pairs and negligible contributions from pp or nn pairs, yielding $n_p(k)/n_n(k) = 1$ for $k > k_F$. So for dominance of T=0 pairs, the cross sections in ^{3}He and ^{3}H at $x \gtrsim 1.5$ will be identical, while for the isospin-independent case, the ratio will be $(2\sigma_p + \sigma_n)/(\sigma_p + 2\sigma_n) \approx 1.4$ for kinematics of the proposal, which yield $\sigma_p \approx 0.3\sigma_n$.

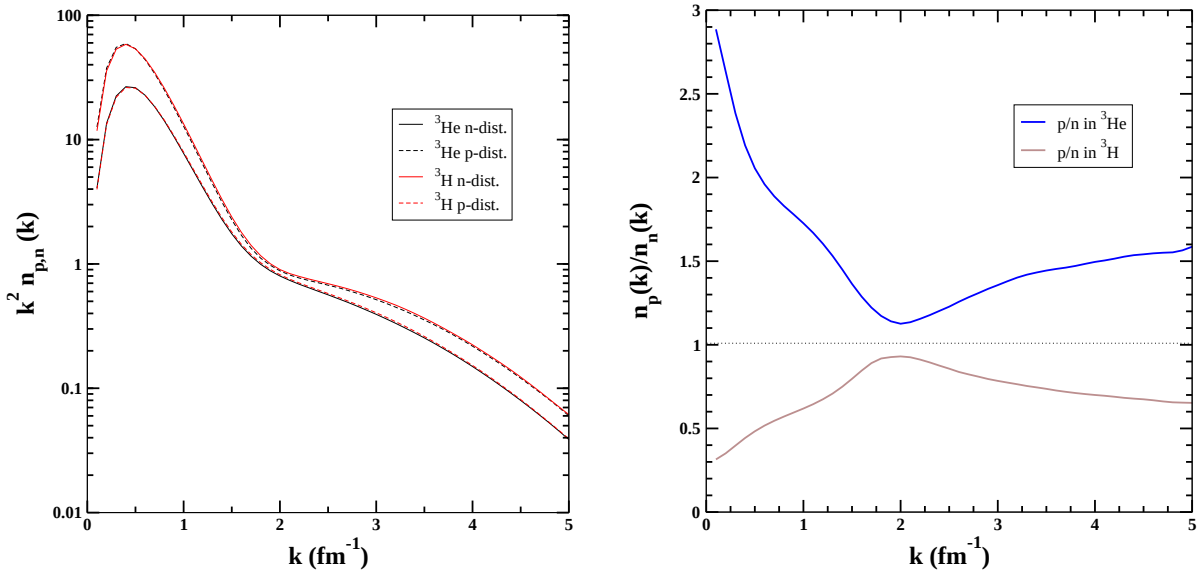

FIG. 6: Left: Momentum distribution for protons (dashed) and neutrons (solid) in ^{3}He (red) and in ^{3}H (black) from Quantum Monte Carlo calculation [14, 15]. Right: Ratio of proton to neutron distributions.

We can also see the impact of the isospin structure of the correlations in the calculated momentum distributions for the proton and neutron in ^{3}He and ^{3}H. Figure 6 shows a calculation of the momentum distribution for protons and neutrons in ^{3}He and ^{3}H, as well as their ratio [14, 15], using the Argonne v18 + Urbana IX two-nucleon and three-nucleon potentials. For the isospin-independent case, the proton-to-neutron ratio would always be Z/N, i.e 2 for ^{3}He and 1/2 in ^{3}H. In the case of dominance of the T=0 np pairs, the ratio in the 2N-SRC dominance region ($k_F < k <$500 MeV/c corresponding to $1.5 < k < 2.5$ fm^{-1} on Fig. 6) would equal 1 in both nuclei. The calculation predicts that the ratio at high momenta, where 2N-SRCs dominate, is well below 2 for ^{3}He. This suggests a significant excess of np pairs over what one would expect from isospin-independent interactions, but not a total dominance of the T=0 pairs. The T=0 pairs dominance is also obvious in Fig. 7 where pn, pp and nn distributions are plotted versus the relative momentum k for a total pair momentum equal to zero, which corresponds to the two nucleons of the pair moving back to back.

A calculation from M. Sargsian [16] was performed at the lowest Q^2 of our proposed experiment using the AV18/UIX

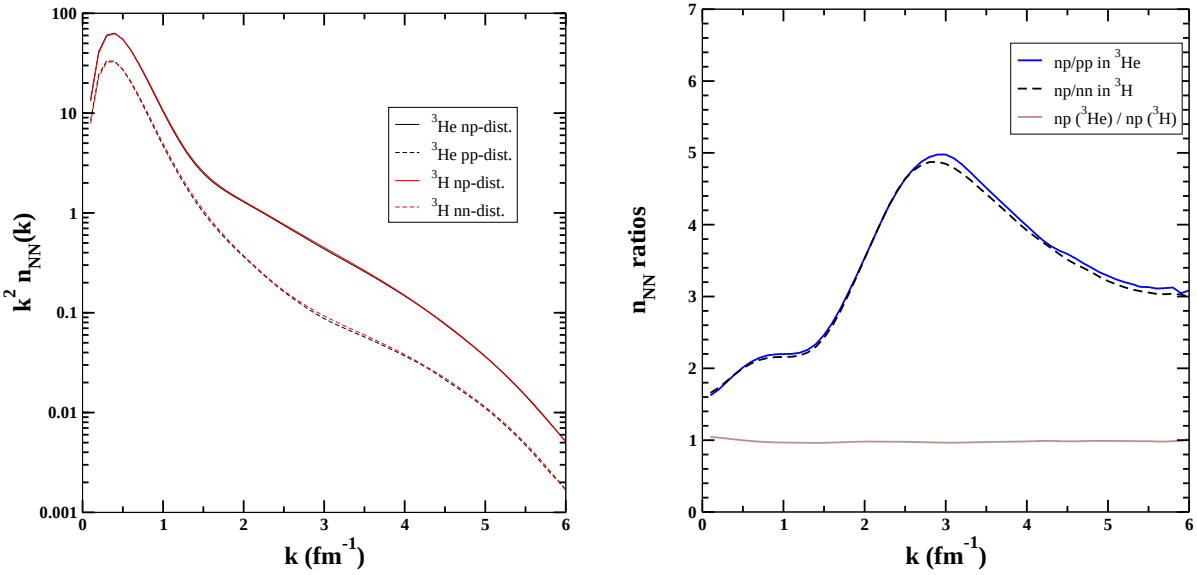

FIG. 7: Left: Momentum distribution of the nucleon np-pair (solid) and nn or pp (dashed) in ^{3}He (black) and ^{3}H (red) as a function of the relative momentum between the two nucleons from Quantum Monte Carlo calculation [14, 15]. Right: Ratio of pn to pp (or nn) distributions. Also plotted is the ratio of the pn distribution in ^{3}He to pn distribution in ^{3}H.

2N and 3N potentials. Inclusive cross sections for ^{3}He and ^{3}H and their ratio are shown on Fig. 8. Above $x \sim 1.4$, the ratio exibits a plateau with the value $\sigma(^3He)/\sigma(^3He) = 1$. This calculation confirms that the scaling regime is reached at $Q^2 \sim 1.5$ (GeV/c)^2 and that the 2N-SRC are strongly isospin-dependent.

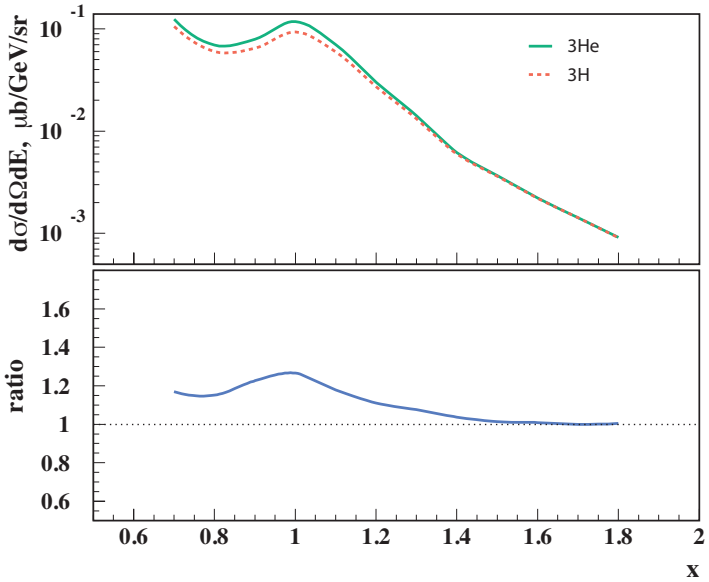

FIG. 8: Calculation from [16]. Top plot: ^{3}He (solid green) and ^{3}H (dashed red) cross sections calculated using AV18/UIX. Bottom plot: ^{3}He/^{3}H cross section ratio (solid blue) for our lowest proposed Q^2 kinematics.

Clearly, in the case of inclusive electron-nucleus scattering, the optimized choice is to look at the isospin dependence on light mirror nuclei. The 40% difference between $T = 0$ dominance and the isospin-independent case allows an

unambiguous distinction between the two assumptions and a clean measure of the ratio $T = 1/T = 0$. For light nuclei, sophisticated calculations exist and can be compared to our results. The motion of the pair and final state interactions should mostly cancel in the ratio allowing a clean interpretation of our data. This can be studied in the region where 2N-SRCs dominate, as well as the region of 3N-SRC dominance, where more isospin configurations are possible for the 3N overlaps as illustrated on Fig. 9.

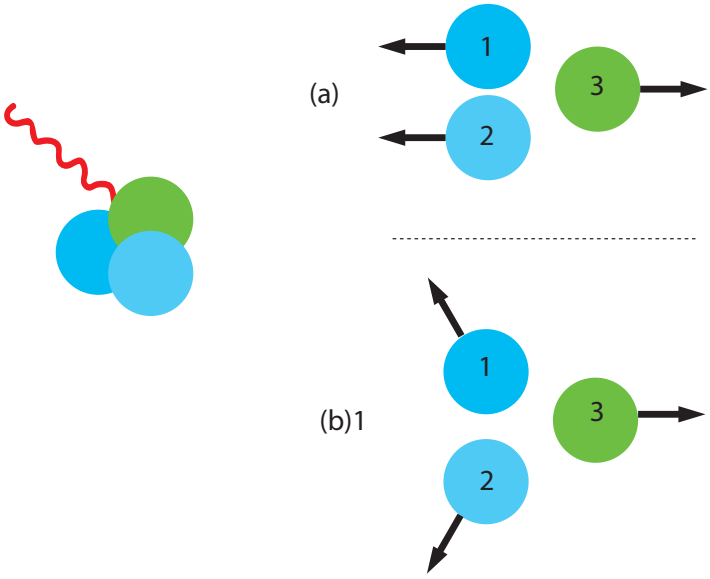

FIG. 9: Illustration of possible 3N-SRC configurations.

In both cases (a) and (b) of Figure 9, the total momentum should be conserved. In the (a)-configuration, two nucleons of the 3N-SRC recoil against the third nucleon inducing an extremely large momentum for the third nucleon: $\|\vec{p_3}\| = \|\vec{p_1}\| + \|\vec{p_2}\|$. However, in the (b)-configuration or "star-configuration", all nucleons of the 3N-SRC have the same momentum: $\|\vec{p_1}\| = \|\vec{p_2}\| = \|\vec{p_3}\|$. Our proposed measurement should be able to differentiate between the momentum ranges implied by these two most probable 3N-configurations.

III. THE PROPOSED MEASUREMENT

Determining the isospin dependence of the short-range correlation pairs and 3N is an important step in the understanding of the strong force at short distances. In order to access the isospin information, we need to choose kinematics in 2N and 3N-SRC regions where scaling has been established. One of the goals of experiment E08-014 [8] is to determine at which Q^2 the cross section ratios at $x > 2.2$ exhibit scaling. In the present proposal, using the results from SLAC and JLab Hall B, we anticipate to be in the correlation scaling regime at Q^2 somewhat above 1.4 (GeV/c)^2. We therefore propose to perform precision measurements of the inclusive electron scattering cross sections for ^{3}H and ^{3}He with an incident beam energy of 4.4 GeV and at two scattering angles: 17.5° and 20°. Our focus is on the $x > 1.25$ region of the 2N- and 3N-SRC plateaus; Fig 10 shows the x and Q^2 coverage of the proposed experiment.

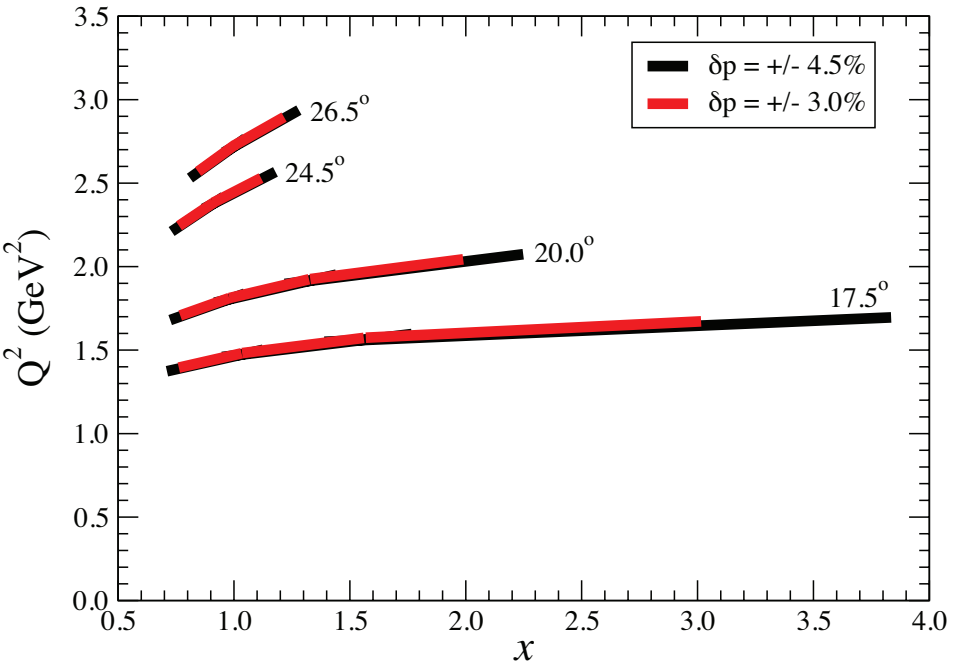

FIG. 10: Kinematic coverage: the black (red) bands represent the full (restricted) acceptance coverage.

We are also planning to take data in the quasi-elastic scattering region scanning a Q^2-range between 1.4 and 2.7 (GeV/c)^2 (the values correspond to the Q^2 at the quasi-elastic peak). At present, the world data for quasi-elastic scattering on ^{3}H has only reached 0.8 (GeV/c)^2 (at the quasi-elastic peak) as shown in Fig. 11.

Finally, taking deuterium data will allow us to directly access spectral functions in the isospin 0 and isospin 1 channels [18]. With ^{2}H, ^{3}H and ^{3}He data taken at the same kinematics, one can form the ratios:

$$\frac{\left[\sigma(^3He) - \sigma(^3H)\right] / \left[\sigma(^3He) + \sigma(^3H)\right]}{\sigma(^2H)}, \tag{3}$$

which directly measures the spectral function of the isospin 1 correlations, and:

$$\frac{\sigma(^3He) - \sigma(^3H)}{\sigma(^2H)}, \tag{4}$$

which directly measures the difference of the spectral functions in I=1 and I=0 channels. Hence, these results will provide, in an independent way, a test of the observation of the small values of the (e,e'pp)/(e,e'pn) ratios.

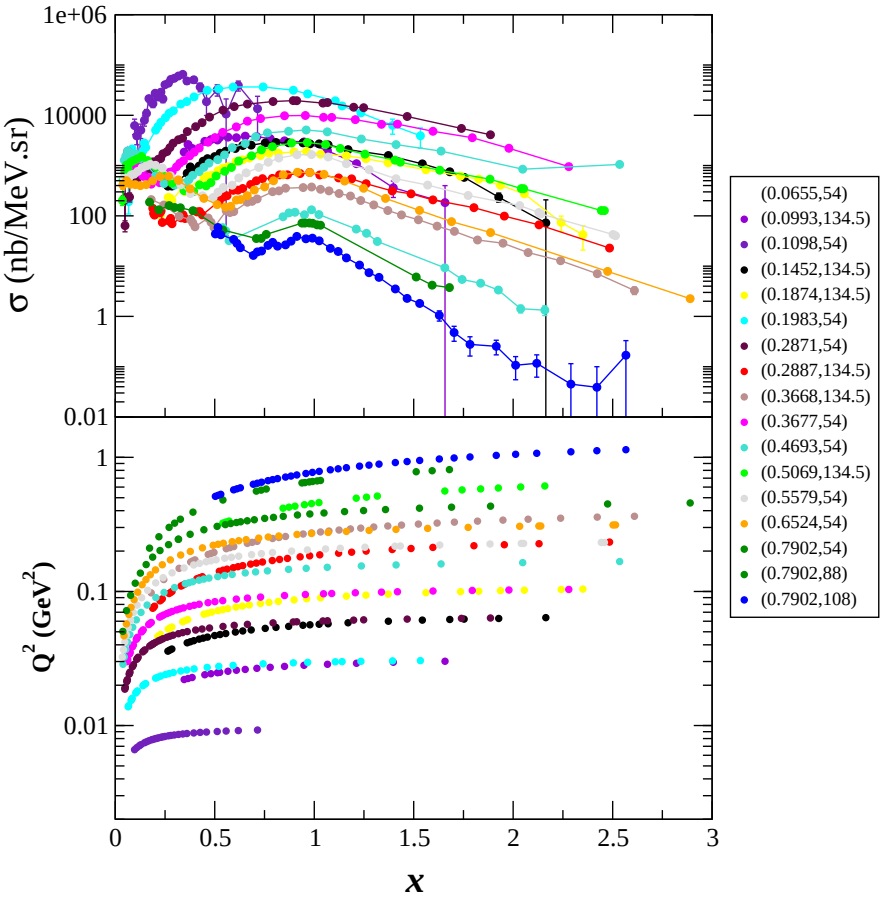

FIG. 11: Existing world data on quasi-elastic scattering off ^{3}H [17]. The legend corresponds to: (incident beam energy in GeV, scattering angle in degree).

We are proposing to divide the experiment in two periods; the first period will include the ^{3}He and ^{3}H targets. The second period will take production data only on deuterium using the same kinematics as the first period.

A. The targets

The ^{3}He and ^{3}H target system has been conditionally approved by PAC30 for the measurement of the ^{3}He and ^{3}H ratio in deep inelastic scattering [19]. At that time, the system considered was using cryogenic targets and therefore high densities (25 mg/cm^2). In an effort to lower the ^{3}H activity, the updated design would be with ^{3}He and ^{3}H gases, contained in identical 40-cm long stainless-steel cans at room temperature and at pressures of 20 and 10 atm, respectively. The diameter of the cell will be 1 cm. Due to welding, the windows and walls are required to be thick and the present design assumes a thickness of 4 mils. In addition, the cell will be placed in another stainless-steel container of same thickness. The space between the can and the container will be filled with hydrogen (H_2) at 9 atm.

The latest density under consideration for the tritium target is 2.5 mg/cm^3 which corresponds to 850 Ci (a factor of 5 reduction compared to [19]). For the ^{3}He target, a density of two times that of tritium would be used.

The target design is presently under study in consultation with engineers at SANDIA National Laboratory, where there is significant experience in handling tritium. More about the safety requirements can be found in Ref. [20].

Finally, we are planning to take data on a 20cm deuterium cryotarget at a later time and also elastic scattering on hydrogen cryotarget for calibration purposes.

B. Background

1. Window contributions to the cross section

Each double window is equivalent to 0.8 times the ^{3}He radiation length. Because the ratios of the ^{56}Fe to ^{3}He cross sections in the 3N-SRC regions are about 4.0 (based on Fig. 3), the stainless steel windows contribution is approximately 6 times the ^{3}He cross section on the ^{3}He target, so dominates the total cross section at x >2. But using the planned 40cm cell and the resolution of the two HRS allows us to perform a software cut to remove the endcap contributions. We also plan to take data on an empty stainless steel can with the same thicknesses to test the efficiency of the cuts, and to subtract any residual endcap contribution.

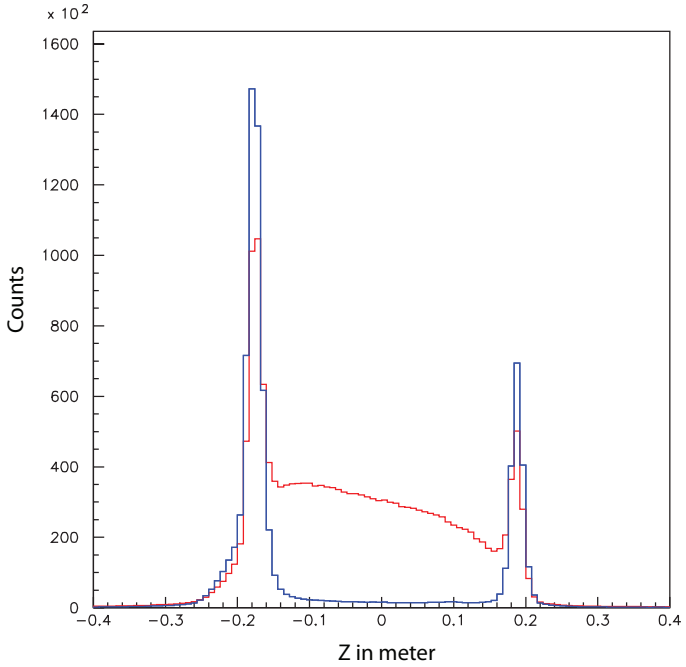

FIG. 12: Projected stainless steel window contributions over the 40cm target length (z). The data are from two runs of E01-012 on the glass reference cell: empty (blue histogram) or filled with ^{3}He (red histogram). The empty reference cell histogram has been scaled to reflect the increase in the window thickness of the assumed target setup.

From previous experiments using 40 cm polarized ^{3}He cells (which have each glass window equivalent to twice the ^{3}He radiation length) and the HRSs, the software cut alone was enough to remove the contribution from the windows [21]. Figure 12 shows data taken during experiment E01-012 in Hall A on the reference cell filled with ^{3}He gas at room temperature and 10.5 atm. In the case of the reference cell, the thickness of the two windows correspond to a total of about 5 times the ^{3}He gas radiation length. In our proposed measurement, we evaluated that the windows will contribute 6 times more than the ^{3}He. Therefore we scaled the empty reference cell data by 6/5 in Fig. 12 to estimate the software cuts we should apply and the remaining window contribution. It should be noted that the data from Fig. 12 were taken at 16° and the vacuum in the empty reference cell wasn't perfect during the run. We can see that a software cut of ±10cm is efficiently removing the window contribution. In our physics rate estimates, an effective target length of about 20cm was used and we considered that 5% of the rates, within the software cuts, will come from the remaining tails of the walls.

Also, depending on the final tritium target system design, the possibility of installing collimators near the target cell might be considered.

2. Pion contamination and charge-symmetric background

The expected pion background has been evaluated using experimental data of JLab Experiment E89-008 [22]. For an incident energy of 4.045 GeV and at a scattering angle of 23°, the π/e ratio was found to be approximately 10:1 for a 2% RL carbon target at a momentum setting of 3.76 GeV and 4:1 for a 2% RL iron target at 3.60 GeV.

The PID performance of Hall A HRS detectors has been shown to be very good in past experiments (see [21, 23], for example) allowing a reduction of the pion background by a factor of about 10^4, while keeping an electron efficiency better than 99%, when a CO_2 gas Čerenkov counter and double-layer lead glass calorimeter are associated. This yields a worst-case pion contamination of ≈0.1%.

The charge-symmetric background can be very large for large scattering angles, but decreases rapidly at smaller angles. For E02-019 [24], the charge-symmetric background for even the high-Z, 6% radiation length targets was always well below 1% for angles below 30° and relatively large values of x ($x \gtrsim 0.6$). For the targets proposed here and scattering angles below 25°, we expect a maximum charge-symmetric background to be below 0.1%.

C. Projected results

To estimate the coverage and the precision of the proposed measurements, a conservative momentum bite of ±3% was used. This is sufficient to fully cover the 3N-SRC region in one setting, although using the full HRS momentum acceptance will improve the coverage in the 2N-SRC region and also expand to the x>3 region (see Fig. 10). The data were binned in x with a binsize of 0.1. The rates for ^{3}He were evaluated using a model based on the data of Ref. [24] on y-scaling for the large x region. This model ("XEM model") was fitted to data on a variety of light and heavy nuclear targets for both the DIS and $x > 1$ region, but with a beam energy of 5.8 GeV.

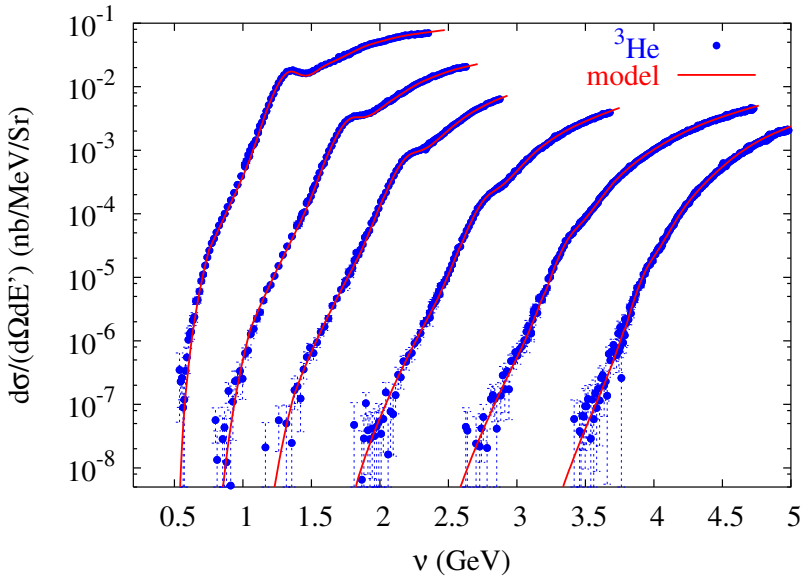

FIG. 13: Comparison of the XEM cross section model for ^{3}He with recent Hall C data [24]. These data cover a Q^2 range between approximatively 2 and 8 (GeV/c)^2 in the quasi-elastic region. The cross section spectrum at the lowest ν is in our proposed Q^2 range of 2 (GeV/c)^2.

Figure 13 shows a comparison of the model with the data from experiment E02-019 [25] from which the XEM model was generated. Also shown in Fig. 14 is a comparison with existing world data on quasi-elastic scattering ^{3}He and

^{3}H [26] at lower Q^2. At these lower Q^2 values, the model is still in good agreement with the data from SLAC [27] and from MIT Bates Linear Accelerator Center [17]. While the model is fitted to the E02-019 kinematics (2–8 GeV^2 in the quasi-elastic region)), it is good at approximately the 20% level down to Q^2 values below 0.5 GeV^2 based on a comparison to the database [26] and also at higher Q^2 values in the resonance region between 1.0 and 4.0 GeV^2 [21].

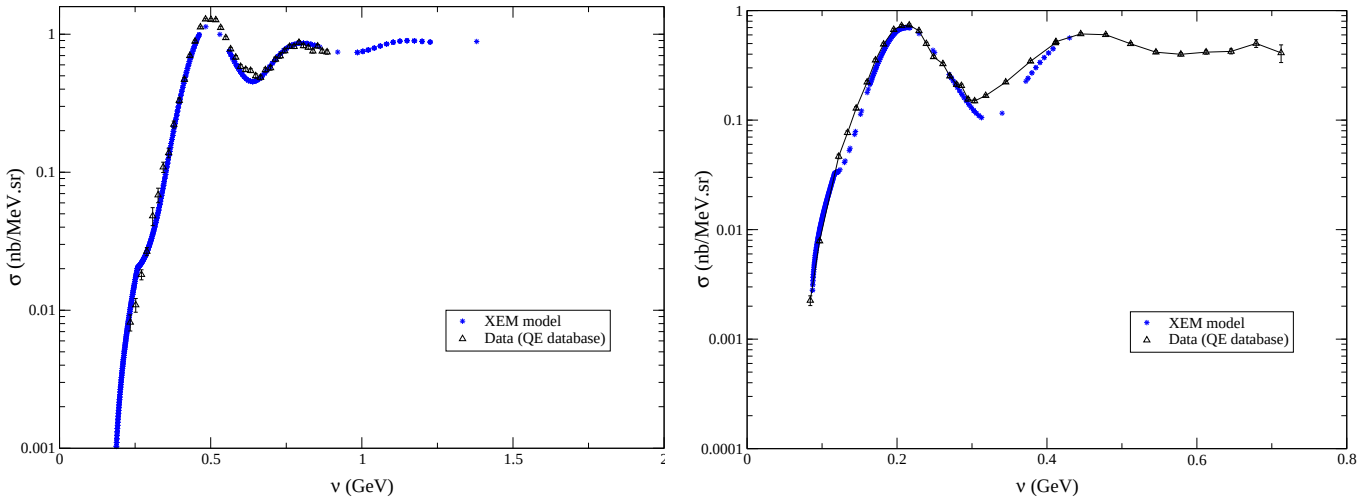

FIG. 14: Comparison of the XEM cross section model with world data [26]. Left plot: ^{3}He at incident energy 3.9 GeV and scattering angle 15° ($Q^2 \approx 0.9$ (GeV/c)^2). Right plot: ^{3}H at incident energy 0.79 GeV and scattering angle 54° ($Q^2 \approx 0.4$ (GeV/c)^2).

The angular acceptance $\Delta\Omega$ was estimated at 3.2msr to maintain good acceptance for long target, with a conservative momentum bite ΔP of ±3% and an effective target length corresponding to a y_{target} cut of ±3.0cm were chosen to evaluate the physics rates. This cut on the target length yields an effective target length of 20cm at 17.5° and 13cm at 26.5°). Runtimes were increased by 20% to account for tracking efficiency and for excess counts from the remaining cell window contribution. The estimated time needed at each kinematic setting is given in Table I, as well as the beam currents (I), the total rates (R_{tot}) after prescaling by the factor psc (also listed) and the physics rates (R_{phys}).

θ (deg)	E' (GeV)	x_{range}	Q^2_{range} (GeV/c)^2	Tg	I (μA)	psc	R_{tot} (Hz)	R_{phys} (Hz)	time (hrs)	Total (hrs)
17.5	3.985	1.6-3.0	1.57-1.67	^{3}He	30	1	427	2.0	40.0	
				^{3}H	30	1	403	0.8	106.7	**146.7**
17.5	3.750	1.0-1.6	1.48-1.57	^{3}He	30	2	2344	90	2.0	
				^{3}H	30	2	1935	33	5.3	
				^{2}H	30	7	3470	398	0.8	**8.1**
17.5	3.530	0.8-1.0	1.40-1.48	^{3}He	30	4	2915	136	2.0	
				^{3}H	30	3	3254	72	4.1	
				^{2}H	30	16	3407	537	0.7	**6.8**
20.0	3.740	1.3-2.0	1.93-2.04	^{3}He	30	1	284	2.2	15.0	
				^{3}H	30	1	258	0.8	40.0	
				^{2}H	30	1	603	23	1.7	**56.7**
20.0	3.520	0.98-1.3	1.81-1.92	^{3}He	30	1	1980	87	4.0	
				^{3}H	30	1	1611	33	10.7	
				^{2}H	30	4	2757	391	1.6	**16.3**
20.0	3.315	0.77-0.98	1.71-1.81	^{3}He	30	2	2134	91	2.0	
				^{3}H	30	2	1788	38	5.3	
				^{2}H	30	7	3044	409	0.6	**7.9**
							Total time needed (LEFT)			**242.5**
24.5	3.100	0.91-1.1	2.38-2.53	^{3}He	30	1	546	23	16.0	
				^{3}H	30	1	443	9	41.8	
				^{2}H	30	1	3024	402	1.3	**59.1**
24.5	2.920	0.76-0.91	2.24-2.38	^{3}He	30	1	1016	33	10.0	
				^{3}H	30	1	861	15	23.1	
				^{2}H	30	2	2553	281	1.5	**34.6**
26.5	3.040	1.0-1.2	2.73-2.90	^{3}He	30	1	184	6.9	28.0	
				^{3}H	30	1	149	2.7	74.7	
				^{2}H	30	1	1078	121	2.8	**105.5**
26.5	2.865	0.85-1.0	2.57-2.73	^{3}He	30	1	414	16	12.0	
				^{3}H	30	1	342	6.7	30.6	
				^{2}H	30	1	2276	262	0.9	**43.5**
							Total time needed (RIGHT)			**242.7**

TABLE I: List of kinematics for left and right HRS and estimated beam time needed for the proposed experiment. The right HRS running is simultaneous to the left HRS running, and so does not increase the total time needed.

The projected precision of our measurements in the 2N-SRC and 3N-SRC regions is shown in Fig. 15. Also drawn are the two cross section ratio predictions from the two isospin dependence assumptions. After combining of statistical and systematic uncertainties (see Table II), it is clear that the sensitivity of our data will allow us to favour one or the other isospin dependence assumption of the pair in the 2N-SRC. Our expected total uncertainty in the 2N-SRC region is about 3%, which will provide a factor of 3-4 improvement of the isospin-dependence measurement compare to the results of Ref. [10]. In addition, we will pioneer the study of the isospin dependence of the 3N-SRCs with

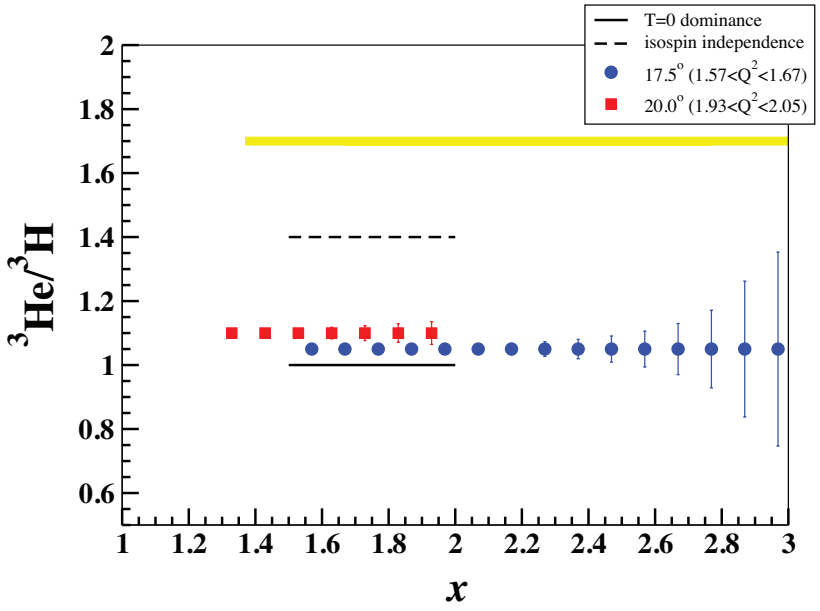

FIG. 15: Projected statistical uncertainties for data taken at a beam energy of 4.4 GeV and at the 2 scattering angles. The yellow bands represent a point-to-point systematic uncertainty of ±1.2%. The error band does not include the overall normalization uncertainty of 2.1%, dominated by the uncertainty in the relative target thicknesses. The dashed black line indicates the prediction assuming that the cross section simply differs by the difference in proton and neutron cross sections. The solid line represents the case where the cross section in the 2N-SRC region is dominated by pn pairs.

relatively precise data at $x > 2.2$.

The statistical projections of our proposed quasi-elastic scattering measurements on ^{3}He and ^{3}H are shown in Fig. 16. From the world data [26], the highest Q^2 reached in quasi-elastic scattering off ^{3}H is about 1.0 (GeV/c)^2. Our proposed measurements are at Q^2 between 1.4 and 2.7 (GeV/c)^2, which can be of great interest for few-body calculations.

Finally, measurements of the absolute cross section for ^{3}H and ^{3}He as $x \to 3$ will provide additional information that can be used to study the impact of final state interactions on inclusive cross section in the region dominated by SRCs. While FSI are expected to be limited to interactions between the nucleons in the SRC, and thus cancel in the target ratios, this assumes that there is no isospin dependence in the FSI. Thus, comparisons to cross section calculations using realistic ^{3}He and ^{3}H distributions will allow us to determine the size of FSI, or else to set limits on their size.

D. Overhead time

The total overhead time needed for calibration, background study and configuration changes is provided below.

Calibration and background studies

We will need to measure the contributions from the stainless-steel entrance and exit windows of the target can. For each kinematic, 15% of the ^{3}He running time should be enough to accomplish a precise dummy subtraction. The

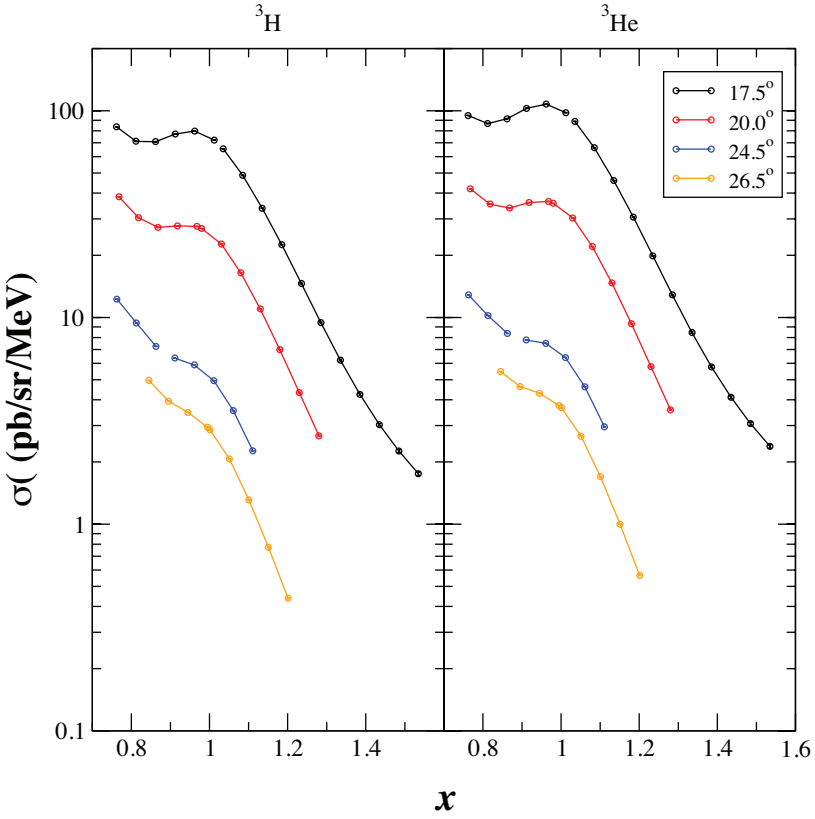

FIG. 16: Projected statistical uncertainties for data taken in the quasi-elastic scattering region at a beam energy of 4.4 GeV and scattering angles of 17.5, 20.0, 24.5 and 26.5°. A relative systematic uncertainty of ±4.6% should be considered for all these data.

time needed for dummy stainless-steel running is about 10 hours. We will also perform the same measurement for the aluminum window contribution to the deuterium cross section and about a hour of beamtime is required.

A beam energy measurement (2 hrs) and BCM calibrations (2 hrs) will be necessary for each running period. We will take optics data at each scattering angle. A 30 minute run on carbon foils for each angle will be sufficient.

For both parts of the experiment, we assume 8 hours for initial checkout. We plan to take elastic hydrogen data at each proposed scattering angle. An hour for each angle should be enough for a total of 2 hours (left and right HRSs running simultaneously).

Also we will conduct careful target boiling and rate dependence studies and ask for 12 hours (8 hours) of beamtime for the first (second) running period.

Configuration changes

We assume 30 minutes for a change of kinematic and 10 minutes for a target motion.

The total overhead for both parts of the experiment are summarized in Table III.

Systematic	$\delta\sigma/\sigma$	$\delta R/R$ (normalization)	$\delta R/R$ (pt-to-pt)
Acceptance correction	2.0%*	0.5%	1.0%
Radiative correction	3.0%*	0.4%	0.3%
Tracking efficiency	1.0%*	-	0.2%
Trigger efficiency	0.5%*	-	0.1%
PID efficiency	1.5%*	-	0.2%
Target thickness	2.0%	2.0%	-
Charge measurement	0.5%	-	0.5%
Energy measurement	0.05%	-	-
COMBINED UNCERTAINTY	4.6%	2.1%	1.2%

TABLE II: Relative systematic uncertainties in the extraction of the unpolarized cross sections from E01-012 [21] and of the cross section ratio from E03-103 [28]. Entries with an asterisk indicate corrections made directly on the cross section. Entries without asterisk indicate contributions to the overall uncertainty. For the target ratios, the acceptance correction is dominated by the target length acceptance, so a 0.5targets.

	1st period ^{3}He + ^{3}H	2nd period ^{2}H + H
Conf change	5 × 0.5hr	4 × 0.5hr + 2 × 0.5hr
Target motion	6 × 3 × 10min	5 × 2 × 10min
H-elastic	0	2 × 1hr
Optics	2 × 0.5hr	2 × 0.5hr
Dummy run	10hr	∼ 1hr
BCM calibration	2 × 1hr	2 × 1hr
Energy measurement	1 × 2hr	1 × 2hr
Boiling study	8hr	4hr
Rate-dependence tests	4hr	4hr
Intial checkout	8hr	8hr
TOTAL	40.5	28.7

TABLE III: Summary of the overhead time needed for the two running periods.

IV. EXPERIMENTS WITH SIMILAR PHYSICS GOALS

This proposal is a logical follow-up of E08-014, approved by PAC33, which will perform a Q^2-scan in the 2N and 3N-SRC in order to determine the onset of scaling and help in the establishment of more relevant scaling variables for the correlation region. E08-014 will also look for the first time at the isospin dependence of the SRCs by taking data on ^{40}Ca and ^{48}Ca. Due to the large atomic number of these isotopes, the results won't be as sensitive to the isospin assumption as in our proposed ^{3}He/^{3}H measurement. Also using light nuclei has the advantage to be compared to realistic calculations. Our ^{3}He/^{3}H measurement is complementary to two-nucleon knockout measurements, such as the completed experiment E01-015 [10] and E07-006, approved by PAC31. The inclusive measurements can be combined with the two-nucleon knockout measurements to better study the relative contributions of 2N- and 3N-SRCs [12], as well providing additional information on the isospin dependence of 2N-SRCs.

The effort in the 12 GeV experiment E12-06-105 is heavily weighted toward very large momentum transfers in an attempt to measure the quark distribution functions in nuclei. It will include measurements of cross sections and ratios for $x > 1$ and will be able to reach higher Q^2 for the 3N-SRC and 4N-SRC regions for several light and heavy

targets.

V. REQUEST TO THE LABORATORY

We are requesting 313 hours (about 13 days) of beam time which will be splitted in two running periods. The first period running ^{3}He and ^{3}H will require 237 hours for the main data taking, 41 hours for configuration changes, calibration, checkout, and background runs. The second period will require take a total of 35 hours for production data, H elastic scattering, configuration changes, calibration, checkout, and background runs. All times assume 100% running efficiency. To achieve our physics goal, we will use the same target design and setup as the conditionnally approved 12 GeV experiment E12-06-118 [19]: 40cm ^{3}H and ^{3}He gas targets, an empty cell and the multi-foil optics targets. For the second running period, we will run with the standard deuterium and hydrogen cryotargets. We will run with the HRS spectrometers using standard dectector packages.

VI. RESOURCES

The Medium Energy Physics group at Argonne National Laboratory has already declared commitment to part of the design and construction of the tritium target system for the "conditionally approved" experiment E12-06-118 [19].

The collaboration is also expected to make major contributions in the upgrade of Hall A beamline for various approved 12 GeV proposals.

---

[1] L. Lapikas, Nucl. Phys. **A553**, 297c (1993).
[2] L. L. Frankfurt and M. I. Strikman, Nucl. Phys. **B181**, 22 (1981).
[3] L. L. Frankfurt and M. I. Strikman, Phys. Rept. **160**, 235 (1988).
[4] C. C. degli Atti and S. Simula, Phys. Lett. B **325**, 276 (1994).
[5] L. L. Frankfurt, M. I. Strikman, D. B. Day, and M. Sargsian, Phys. Rev. C **48**, 2451 (1993).
[6] K. S. Egiyan et al. (CLAS), Phys. Rev. C **68**, 014313 (2003).
[7] K. S. Egiyan et al. (CLAS), Phys. Rev. Lett. **96**, 082501 (2006).
[8] P. Solvignon, J. Arrington, D. B. Day, D. Higinbotham, et al., Jefferson Lab experiment E08-014.
[9] A. Tang et al., Phys. Rev. Lett. **90**, 042301 (2003).
[10] R. Shneor et al. (Jefferson Lab Hall A), Phys. Rev. Lett. **99**, 072501 (2007).
[11] W. Bertozzi, E. Piasetzky, J. Watson, S. Wood, et al., Jefferson Lab experiment E01-015.
[12] E. Piasetzky, M. Sargsian, L. Frankfurt, M. Strikman, and J. W. Watson, Phys. Rev. Lett. **97**, 162504 (2006).
[13] R. Schiavilla, R. B. Wiringa, S. C. Pieper, and J. Carlson, Phys. Rev. Lett. **98**, 132501 (2007).
[14] S. C. Pieper and R. B. Wiringa, Ann. Rev. Nucl. Part. Sci. **51**, 53 (2001), nucl-th/0103005.
[15] B. Wiringa, private communication.
[16] M. M. Sargsian, private communication.
[17] K. Dow et al., Phys. Rev. Lett. **61**, 1706 (1988).
[18] M. I. Strikman, private communication.
[19] G. Petratos, J. Gomez, R. Holt, R. D. Ransome, et al., Jefferson Lab proposal E06-12-118 (conditionally approved).
[20] **DOE HANDBOOK:** *tritium handling and safe storage* (March 2007), DOE-HDBK-1129-2007.
[21] P. Solvignon, Ph.D. thesis, Temple University (2006).
[22] J. Arrington et al., Phys. Rev. Lett. **82**, 2056 (1999).
[23] J. Alcorn et al., Nucl. Inst. & Meth. **A522**, 294 (2004).
[24] N. Fomin, Ph.D. thesis, University of Virginia (2008).
[25] J. Arrington, D. Day, B. Filippone, A. F. Lung, et al., Jefferson Lab experiment E02-019.
[26] O. Benhar, D. Day, and I. Sick (2006), nucl-ex/0603029.
[27] Z. E. Meziani et al., Phys. Rev. Lett. **69**, 41 (1992).
[28] J. Seely, Ph.D. thesis, Massachusetts Institute of Technology (2006).